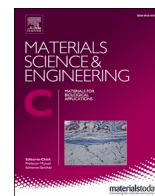




Since January 2020 Elsevier has created a COVID-19 resource centre with free information in English and Mandarin on the novel coronavirus COVID-19. The COVID-19 resource centre is hosted on Elsevier Connect, the company's public news and information website.

Elsevier hereby grants permission to make all its COVID-19-related research that is available on the COVID-19 resource centre - including this research content - immediately available in PubMed Central and other publicly funded repositories, such as the WHO COVID database with rights for unrestricted research re-use and analyses in any form or by any means with acknowledgement of the original source. These permissions are granted for free by Elsevier for as long as the COVID-19 resource centre remains active.



On the importance of physicochemical parameters of copper and aminosilane functionalized mesoporous silica for hydroxychloroquine release

Anna Olejnik^{*}, Joanna Goscińska^{*}

Adam Mickiewicz University in Poznań, Faculty of Chemistry, Department of Chemical Technology, Uniwersytetu Poznańskiego 8, 61-614 Poznań, Poland

ARTICLE INFO

Keywords:

Mesoporous materials
Surface modification
Impregnation
Drug release
Release kinetics

ABSTRACT

Recently, great attention has been paid to hydroxychloroquine which after promising *in vitro* studies has been proposed to treat the severe acute respiratory syndrome caused by SARS-CoV-2. The clinical trials have shown that hydroxychloroquine was not as effective as was expected and additionally, several side effects were observed in patients cured with this medicament. In order to reduce them, it is suggested to deliver hydroxychloroquine in a controlled manner. Therefore, in this study non-modified (SBA-15, SBA-16) and modified with copper and aminosilane mesoporous silica materials were applied as novel nanocarriers for hydroxychloroquine. First, pristine and functionalized samples were synthesized and characterized by X-ray diffraction, low-temperature nitrogen sorption, transmission electron microscopy, X-ray photoelectron spectroscopy, infrared spectroscopy, laser diffraction. Then the influence of physicochemical parameters of materials obtained on the adsorption and release processes of hydroxychloroquine was analyzed. The mechanism of hydroxychloroquine binding to non-modified silicas was based on the formation of hydrogen bonds, while in the case of copper and aminosilane functionalized materials the complexes with drug molecules were generated. The release behavior of hydroxychloroquine from silica samples obtained was determined by different factors including pH conditions, textural parameters, surface charge, and presence of surface functional groups. The greatest differences in hydroxychloroquine release profiles between materials were observed at pH 7.2. The amount of drug desorbed from silica decreased in the following order: functionalized SBA-15 (84%) > functionalized SBA-16 (79%) > SBA-15 (59%) > SBA-16 (33%). It proved that a higher amount of drug was released from materials of hexagonal structure.

1. Introduction

Hydroxychloroquine sulfate (HCQ) is a drug applied to treat malaria, discoid lupus erythematosus, and autoimmune diseases including rheumatoid arthritis, antiphospholipid syndrome, Sjogren's syndrome [1–4]. Long-term application of HCQ is often recommended for patients who suffer from cutaneous lupus and systematic lupus erythematosus (SLE) [5]. Hydroxychloroquine sulfate exhibits a beneficial outcome on SLE because it reduces the impact of the risk related to thrombotic effects and organ destructions [6]. It was proved that both chloroquine and its hydroxy-derivative HCQ indicate positive effects in reducing viral replication and prevent its fusion to cell membranes [7,8]. According to previous studies these compounds showed antiviral activity against the Ebola virus [9], Zika virus [10], Human Immunodeficiency Virus (HIV-1) [11], poliovirus [12], hepatitis A and C [13], and SARS-CoV-1 [14]. In recent times, HCQ was also proposed to treat the

severe acute respiratory syndrome caused by coronavirus-2 (SARS-CoV-2) in the reference to the promising *in vitro* studies. This drug was applied alone or in combination with azithromycin in hospitals and primary care practices [15,16]. Currently, more than 200 trials of hydroxychloroquine/chloroquine or both and in connection with other medicaments are registered globally. It was reported that hydroxychloroquine improved outcomes in a small number of patients infected with coronaviruses [17]. However, the efficacy of HCQ was not as good as it was expected. The results proved that the treatment with HCQ of adults suffered from COVID-19 did not ameliorate the clinical status of the patient compared with placebo [18]. It was shown that hydroxychloroquine neither increased nor reduced the risk related to intubation or death in the case of COVID-19 [19].

From a chemical point of view, HCQ is an aminoquinoline that has an amino group attached to a quinoline ring and it contains a hydroxyl group at the N-ethyl end (Table 1). Hydroxychloroquine sulfate is a less

^{*} Corresponding authors.

E-mail addresses: annamar@amu.edu.pl (A. Olejnik), asiagosc@amu.edu.pl (J. Goscińska).

<https://doi.org/10.1016/j.msec.2021.112438>

Received 15 May 2021; Received in revised form 29 August 2021; Accepted 12 September 2021

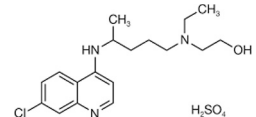
Available online 17 September 2021

0928-4931/© 2021 The Author(s).

Published by Elsevier B.V. This is an open access article under the CC BY-NC-ND license

(<http://creativecommons.org/licenses/by-nc-nd/4.0/>).

Table 1
Hydroxychloroquine – chemical structure and geometric properties (Spartan '18. Version 1.4.5. Jun. 29. 2020).

Structure	MW (g/mol)	Area (Å ²)	Volume (Å ³)	Polar surface area (Å ²)	Ovality
	434	461.38	413.85	114.076	1.72

toxic derivative of chloroquine that has an additional hydroxyl group. HCQ sulfate is available as film-coated tablets for oral administration (200 mg of the active ingredient is used per tablet). Dosage applied is different depending on the treatment indication. Hydroxychloroquine is absorbed within 2 to 4 h after oral administration [20] in the upper part of the intestinal tract. HCQ is metabolized in the liver by cytochrome *p*450 [21] and 3 metabolites such as desethylchloroquine, desethylhydroxychloroquine and bisdesethylhydroxychloroquine are formed [22] that also exhibit pharmacological activities. Afterward, the metabolized and unchanged hydroxychloroquine is expelled through urine or excrement. In general, HCQ presents a good safety profile, however, it also exhibits some negative effects. The most common one is associated with gastrointestinal disorders such as retch, vomiting, and diarrhea [23]. Application of HCQ can cause arrhythmia, myopathy, and prolonged QT interval that corresponds to the abnormal pattern observed on the electrocardiogram that is related to a high risk of sudden cardiac death. However, the most complex toxicity of HCQ is the development of retinopathy, which is associated with irreversible visual loss [24]. Moreover, wide application of hydroxychloroquine may cause cutaneous adverse reactions and hepatic failure [25]. HCQ can have also other side effects such as hair loss, hives, bronchospasm, muscle weakness, and unusual bleeding or bruising. Additionally, the reports proved that the treatment with hydroxychloroquine may induce the exacerbation of psoriasis [26].

In order to reduce the side effects of HCQ and to deliver this drug in a controlled manner, it is proposed to apply nanocarriers. So far ordered mesoporous silica (OMS) have been utilized as vehicles for various active compounds [27–29]. Due to their nontoxicity, high stability, well-developed surface area and great pore volume mesoporous silica can be recommended as an ideal candidate for drug hosting. Recently, hollow mesoporous silica spheres with polyelectrolyte multilayers have been applied as a delivery system for ibuprofen [29]. In another study biomimetic diselenide-bridged mesoporous organosilica nanoparticles were used as a carrier for doxorubicin in chemotherapy [30]. This drug was also delivered by using mesoporous silica nanoparticles conjugated with TAT peptide [31]. The presence of silanol groups on their surface enables to perform their modification using various organic groups. The introduction of amino-functional groups may enhance the sorption abilities of materials while the presence of copper may generate acid-base active centers on the surface of materials. It should be also highlighted that at trace concentrations copper is curial for life and takes part in enzymatic reactions in humans [32]. Moreover, copper exhibits antiviral and antibacterial activity [33–35], therefore the impregnation of mesoporous materials with copper(II) chloride is fully justified. So far colloidal silica was applied as an excipient for HCQ [36]. In another study, hydroxychloroquine-loaded hollow mesoporous silica nanoparticles (HMSN) were obtained to increase the therapeutic effectiveness of radiotherapy in cancer treatment. It was proved that HMSN accelerated the drug delivery to tumors and inhibited their growth [37]. However, there are no literature data concerning the application of modified OMS as carriers for hydroxychloroquine sulfate. Therefore, the aim of this study is to assess the importance of physicochemical properties of copper and aminosilane functionalized OMS during the adsorption and release of HCQ sulfate.

1. Materials and methods

1.1. Synthesis and modification of mesoporous materials

1.1.1. SBA-15

Firstly, 10 g of triblock copolymer Pluronic P123 (Sigma-Aldrich) was introduced to the solution of hydrochloric acid (2 M, 70 cm³) and distilled water (150 cm³) stirred on a magnetic stirrer at 55 °C. Next 20 g of tetraethyl orthosilicate (Sigma-Aldrich) was added drop by drop. The components were then stirred at 55 °C for the period of 8 h and afterward dried at 100 °C for 16 h. The material was filtered off and dried. In the last step, the product was calcined at 550 °C for the period of 8 h.

1.1.2. Modification of SBA-15

The SBA-15 material obtained according to the above-presented procedure was functionalized with 3-aminopropyltriethoxysilane (APTES) and in the next step, it was impregnated with an aqueous solution of copper(II) chloride. The modification was performed under reflux. 4 g of SBA-15 was immersed in toluene (347.8 cm³). Next APTES (17.4 cm³) was added while mixing. Afterward, all components were stirred at 100 °C for 24 h. The solvent was removed by hot filtration and the modified silica was dried at 100 °C. Subsequently, an incipient wetness technique was applied to impregnate aminosilane functionalized SBA-15 with an aqueous solution of copper(II) chloride in the amount necessary to obtain 1 wt% Cu loading. For 2 g of functionalized SBA-15, 0.05 g CuCl₂ dissolved in 3 cm³ distilled water was applied. In the last stage of synthesis, the material was dried at 100 °C for 24 h. The SBA-15 materials modified with 3-aminopropyltriethoxysilane and copper are denoted as Cu/SBA-15-AS (AS corresponds to aminopropyltriethoxysilane).

1.1.3. SBA-16

SBA-16 material was obtained by adding 3 g of Pluronic F127 copolymer (Sigma-Aldrich) to the solution of hydrochloric acid (9 cm³) and distilled water (144 cm³). The mixture was then stirred at 35 °C until the copolymer was totally dissolved. Concomitantly, 1-butanol (1 cm³) was introduced, and all components were stirred for 1 h. Afterward, tetraethyl orthosilicate (13.2 g) was added. The mixture was stirred for 24 h at 35 °C and subsequently, it was subjected to hydrothermal treatment for 24 h at 100 °C. The material obtained was filtered off when hot. Then, it was dried, refined, and calcined at 550 °C for 8 h.

1.1.4. Modification of SBA-16

The SBA-16 synthesized based on the above-described method was functionalized with APTES and afterward, it was impregnated with an aqueous solution of CuCl₂. The functionalization process was carried out under reflux. 6.3 g of SBA-16 was introduced to 547.8 cm³ of toluene. Subsequently, 27.4 cm³ of APTES was introduced while stirring and all ingredients were mixed at 100 °C for 24 h. Then toluene was removed by hot filtration and the SBA-16 functionalized with APTES was dried at 100 °C. 2 g of SBA-16 modified with APTES was weighted to perform the impregnation process with CuCl₂. 0.05 g of copper(II) chloride was dissolved in 3 cm³ of distilled water. Next, metal-containing solution was added drop by drop on the surface of functionalized SBA-16. The impregnated sample was dried at 100 °C for 24 h. The SBA-16 materials

modified with 3-aminopropyltriethoxysilane and copper are denoted as Cu/SBA-16-AS (AS corresponds to APTES).

1.2. Sample characterization

1.2.1. Small-angle X-ray scattering (SAXS)

The small-angle X-ray scattering was performed by X-ray diffractometer (Empyrean, PANalytical) with the copper $K\alpha_1$ radiation ($\lambda = 1.5406 \text{ \AA}$) and the copper $K\alpha_2$ radiation ($\lambda = 1.5444 \text{ \AA}$). The step size was 0.0001° .

1.2.2. Powder X-ray diffraction (XRD)

All materials synthesized were characterized by using powder X-ray diffraction (D8 Advance Diffractometer, Bruker, U.S.) with the copper $K\alpha_1$ radiation ($\lambda = 1.5406 \text{ \AA}$). The XRD analyses were performed at room temperature with a step size 0.05° in the high-angle range.

1.2.3. Transmission electron microscopy (TEM)

The samples were placed on a grid with a carbon film and analyzed by transmission electron microscope (JEOL 2000) operating at 80 kV.

1.2.4. Nitrogen sorption

The pore structure of the OMS was determined based on low-temperature nitrogen adsorption-desorption isotherms using a sorptometer Quantachrome Autosorb iQ (U.S.). Before starting the measurements, pristine materials (SBA-15 and SBA-16) were degassed in a vacuum at 300°C for 5 h, while modified OMS samples were degassed at 150°C for 5 h. The surface area and pore size distribution were estimated by BET (Brunauer–Emmett–Teller) and BJH (Barret–Joyner–Halenda) methods. Additionally, average pore diameter and total pore volume were also designated.

1.2.5. Elemental analysis

Elemental composition of materials was determined using Elemental Analyser Vario EL III.

1.2.6. X-ray photoelectron spectroscopy (XPS)

The XPS analyses were performed by an UHV SPECS spectrometer. The experiments were carried out with the use of Al $K\alpha$ radiation by a PHOIBOS HSA3500 analyzer, working in the FAT scan mode with a pass energy of 20 eV. The XPS spectra were recorded and in the next step calibrated by using the C 1s peak at 284.5 eV as an internal standard. Core-level peaks were examined by non-linear Shirley-type background subtraction. The data processing was performed by the CasaXPS program. The accuracy of the binding energy values was assessed to be ± 0.1 eV.

1.2.7. Laser diffraction

Particle size distribution (PSD) of the mesoporous materials was determined by Mastersizer 3000 (Malvern Instruments Ltd., UK). The drop of surfactant (polysorbate 20) was added to OMS in order to prevent their floating in the dispersant. The samples were dispersed in distilled water and put into the hydro dispersion unit. The results were depicted in the form of percentages of $d(0.1)$, $d(0.5)$ and $d(0.9)$ [28]. The data in the form of $d(0.1)$ gives information that 10% of particles have the size smaller than the value obtained, $d(0.5)$ that represents the median of particle sizes and $d(0.9)$ which notifies that 90% of particles have a size smaller than the results received. Additionally, the $D[3.2]$ known as Sauter Mean Diameter enables to monitor the proportion of fine particles in the samples while the $D[4.3]$ recognized as volume moment mean or De Brouckere Mean Diameter reflects the coarse particles in OMC materials.

1.2.8. Zeta potential measurement

The electrokinetic properties of modified and non-modified OMS samples were assessed over pH ranging from 1.5 to 8 by Zetasizer Nano

ZS (Malvern Instruments Ltd., UK) equipped with an auto-titrator. The zeta potential was estimated based on the Henry equation [38].

1.2.9. FT-IR spectroscopy

FT-IR spectra of the OMS before and after HCQ adsorption were registered by using spectrometer (Bruker IFS 66v/S, U.S.). The samples were mixed with anhydrous KBr (1 mg of silica per 200 mg KBr). The infrared spectra were recorded in a wavenumber range of $4000\text{--}400$ cm^{-1} .

1.3. Adsorption of HCQ

In order to perform the adsorption process of HCQ onto OMS materials, series of aqueous drug solutions with concentrations from the range of 6.25 to 125.00 mg/dm^3 were prepared. 0.04 g of each nanomaterial (SBA-15, Cu/SBA-15-AS, SBA-16, and Cu/SBA-16-AS) were suspended in 50 cm^3 of HCQ solutions. As prepared samples were shaken steadily in a shaker (KS 4000i control, IKA, Germany) for 24 h at room temperature. Afterward, the mixtures were filtered off and the concentration of HCQ found in the supernatant liquid was measured at the wavelength of 231 nm by spectrophotometer UV–Vis (Cary 60, Agilent, U.S.). The amount of hydroxychloroquine sulfate adsorbed on the surface of OMS samples was estimated based on the following equation:

$$q_e = \frac{(C_0 - C_e) V}{m} \quad (1)$$

where C_0 represents the initial concentration of HCQ (mg/dm^3). C_e denotes the residual concentration of hydroxychloroquine sulfate (mg/dm^3). V is the volume of HCQ solution (dm^3), and m represents the mass of silica nanomaterial (g).

1.4. Release of HCQ

The release experiments of HCQ from OMS materials were performed in three different conditions to simulate gastric fluid (pH 1.2), intestinal fluid (phosphate buffer of pH 5.8) and saliva (phosphate buffer pH 7.2). The receptor fluids were maintained at $37.0^\circ\text{C} \pm 0.50^\circ\text{C}$ with the stirring of speed 100 rpm. Before the release test, 0.025 g of mesoporous silica materials were added into the 3 cm^3 of HCQ solution (0.005 g of HCQ in 3 cm^3 of distilled water). Afterward, the mixture was placed in a drier for 24 h. When the solvent was evaporated the mesoporous materials loaded with HCQ were dispersed in receptor fluids of different pH. At specified time intervals, the samples were withdrawn and the changes in concentration of HCQ were monitored at the wavelength of 231 nm by UV–Vis spectrophotometer (Cary 60, Agilent, U.S.). The data obtained were then used to quantify the percent of HCQ release *versus* time. The studies were carried out sixfold and both average and standard deviation were calculated. Additionally, the release results were fitted to mathematical kinetic models such as zero-order (Eq. (2)), first-order (Eq. (3)), Higuchi's model (Eq. (4)), Korsmeyer-Peppas model (Eq. (5)), and Hixson-Crowell model (Eq. (6)) [39,40] using following equations:

$$F_t = k_0 t \quad (2)$$

$$F_t = 1 - e^{-kt} \quad (3)$$

$$F_t = k_H \sqrt{t} \quad (4)$$

$$F = (M_t/M) = k_{KP} t^n \quad (5)$$

$$\sqrt[3]{F_0} - \sqrt[3]{F_t} = k_{HC} t \quad (6)$$

Where F_t is the fraction of HCQ released over a certain time, t (h); F_0 is the initial amount (mg) of HCQ in OMS materials, and k_0 , k , k_H , k_{KP} , k_{HC} correspond to release constants of particulate kinetic models.

Furthermore, R^2 was estimated to determine which mathematical model follows the particular release profile.

2. Results and discussion

The structure of OMS materials was assessed by small-angle X-ray scattering (SAXS). Due to the SAXS profiles obtained it was possible to determine if the modification of SBA-15 and SBA-16 using APTES and impregnation with an aqueous solution of copper(II) chloride influenced the structure of newly synthesized materials. The SAXS profiles are depicted in Fig. 1.

Based on the SAXS profiles, it was observed that SBA-15 silica is a material with a highly ordered mesoporous structure (Fig. 1 A). The pattern of SBA-15 contains a characteristic peak of hexagonal pore arrangement detected at 2θ around 1° that corresponds to the plane (100) [41]. Additionally, two peaks were observed at 2θ – 1.7° and 1.9° representing the (110) and (200) planes, respectively [42]. These three well-separated reflections indicate the hexagonal two-dimensional mesoporous structure (space group $P6mm$) [41,43]. The SAXS pattern of Cu/SBA-15-AS (Fig. 1 B) also reveals three characteristic peaks detected at 2θ around 1° , 1.7° and 1.9° . However, their intensity decreased compared to the non-modified material that may indicate a disturbance of the ordered mesoporous structure. The SAXS profile of SBA-16 pristine silica presents reflections corresponding to the planes (110), (200), and (211) that confirm the three-dimensional cubic structure of $Im3m$ space group (Fig. 1 C) [44]. Three characteristic peaks at 2θ around 0.9° , 1.6° , and 2.1° were noticed. The modification of SBA-16 with aminosilane and copper(II) chloride led to a slight reduction in the intensity of reflections. Two peaks were identified at 2θ around 0.9° and 2.1° (Fig. 1 D). The detailed characterization of each peak is presented in Table S1 (Supporting Information).

The XRD profiles of Cu/SBA-15-AS and Cu/SBA-16-AS samples in the high-angle range contain only wide reflections at 2θ – 23° corresponding to amorphous silica. However, no phases derived from modifiers were observed (Fig. 2).

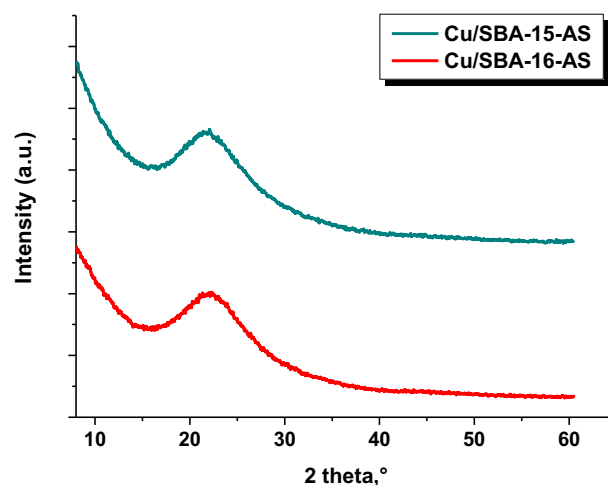


Fig. 2. X-ray diffraction patterns in the high-angle range of the modified OMS: Cu/SBA-15-AS and Cu/SBA-16-AS.

The structure of materials obtained was determined by TEM images which are displayed in Fig. 3. The hexagonal arrangement of pores was observed for both SBA-15 and Cu/SBA-15-AS materials (Fig. 3A, B). In turn, highly ordered cubic structure was detected for SBA-16 before and after functionalization with APTES and copper(II) chloride (Fig. 3C, D). The dark areas in the TEM images represent the walls of the OMS, whereas the white spots reflect the pores of materials. It was observed that the arrangement of pores was partially disturbed for modified silica materials.

The textural parameters including BET surface area, total pore volume, average pore diameter of OMS are collected in Table 2. The pore diameters of all silicas are within the typical range for mesoporous materials from 2 to 50 nm. The highest average pore diameter was observed for Cu/SBA-15-AS while the smallest for SBA-16. Unmodified

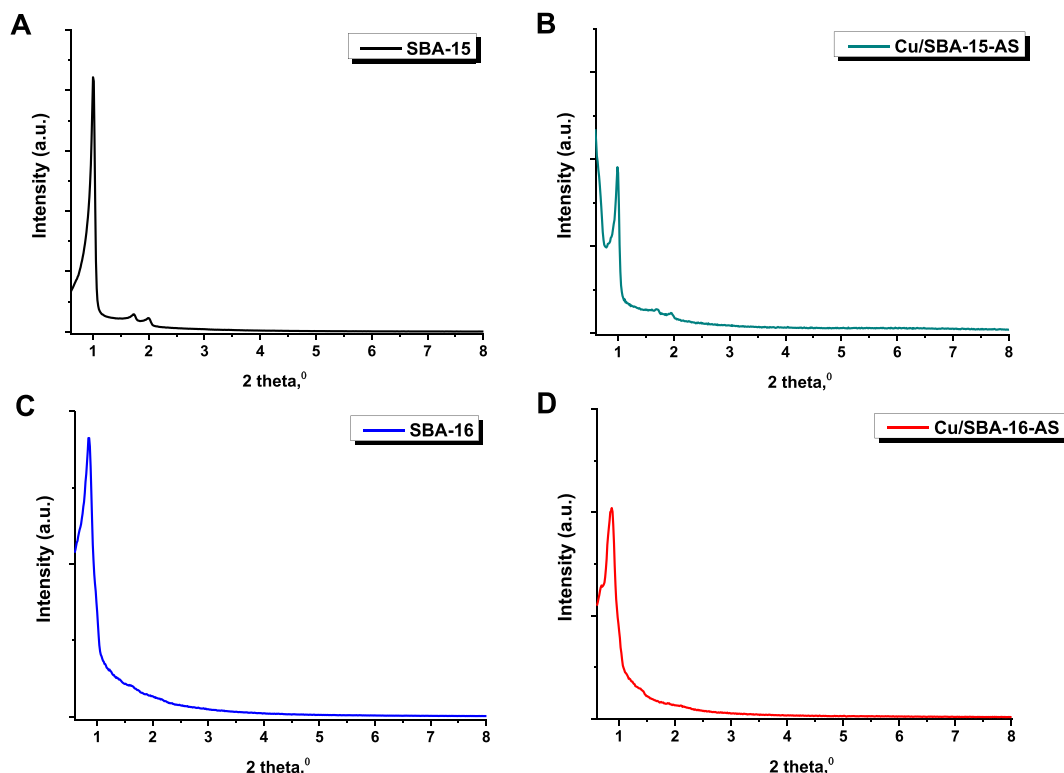


Fig. 1. SAXS profiles of SBA-15 (A), Cu/SBA-15-AS (B), SBA-16 (C), and Cu/SBA-16-AS (D).

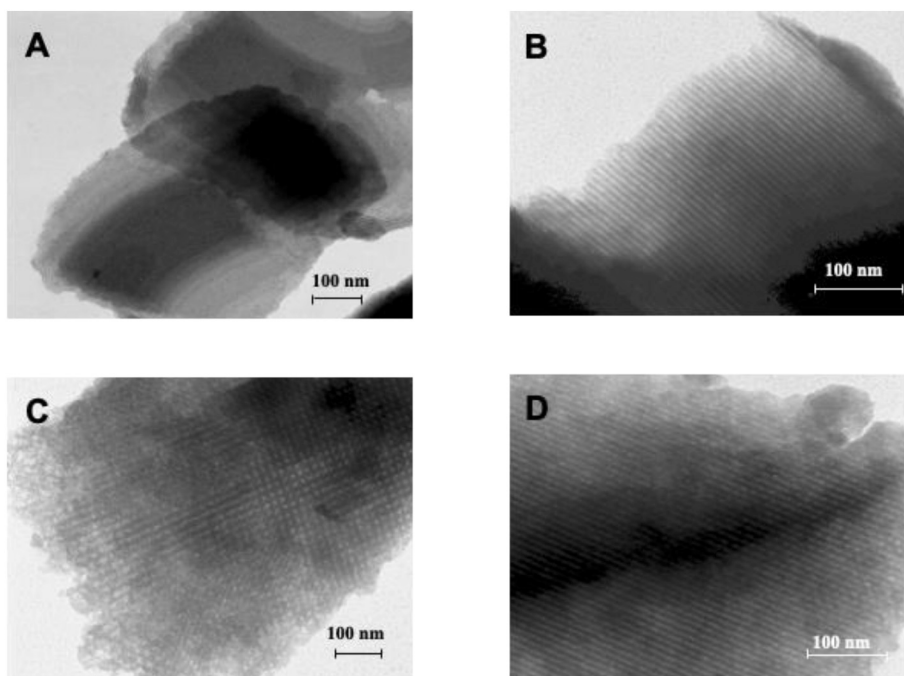


Fig. 3. TEM micrographs of SBA-15 (A), Cu/SBA-15-AS (B), SBA-16 (C), and Cu/SBA-16-AS (D).

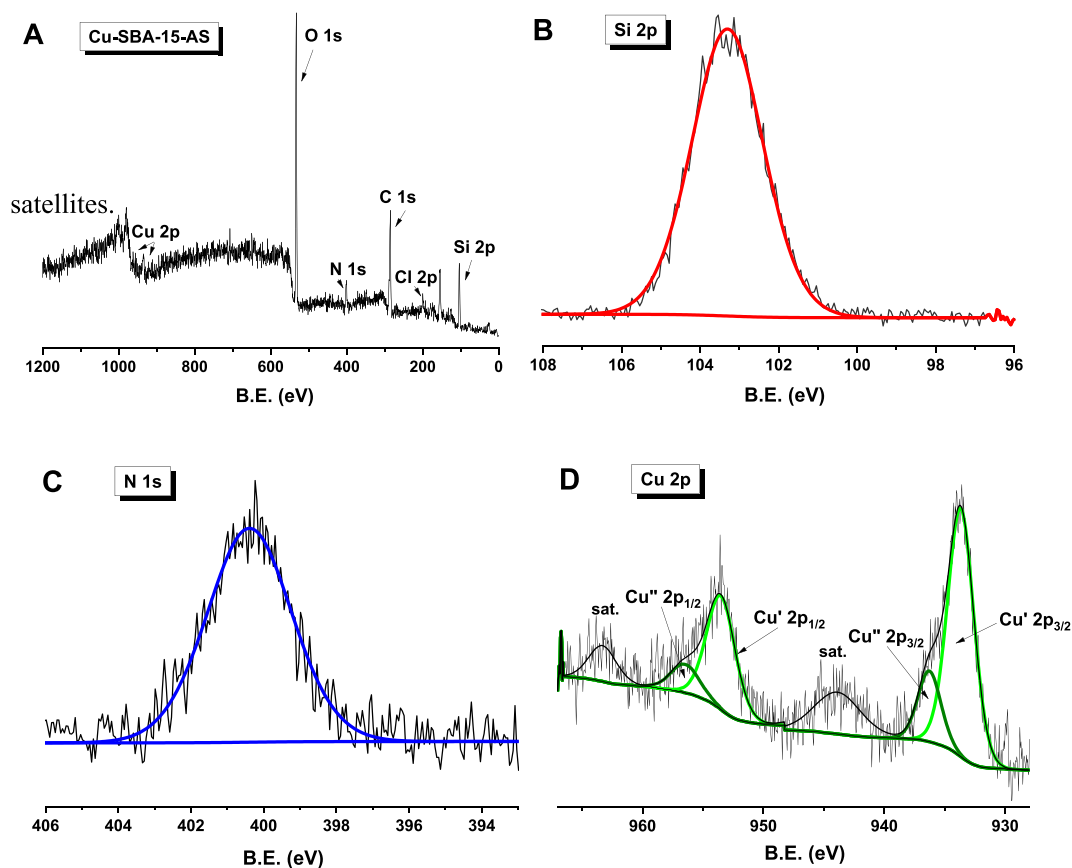


Fig. 4. The XPS spectra of Cu/SBA-15-AS: A) survey spectrum, and high-resolution spectra of B) Si 2p, C) N 1s, D) Cu 2p.

SBA-15 and SBA-16 materials were characterized by a comparable BET surface areas, ranging from 703 to 727 m²/g. The modification of materials with aminosilane and copper(II) chloride led to a decrease in the BET surface area and pore volume for both Cu/SBA-15-AS and Cu/SBA-

16-AS. These results proved that the functional groups were situated not only on the outer surface of materials but also inside the channels of their mesostructures [45]. It is suggested that the modification of silica undergoes more willingly at the micropore or small mesopore openings.

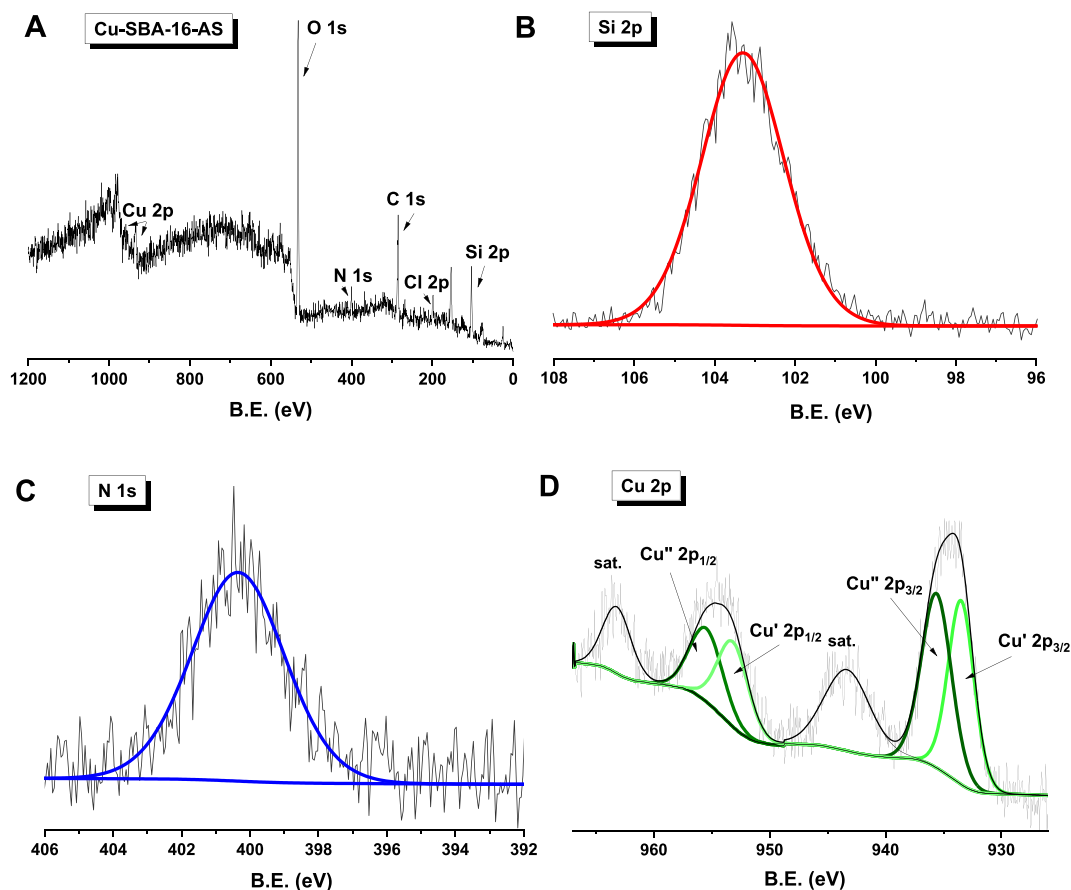


Fig. 5. The XPS spectra of Cu/SBA-16-AS: A) survey spectrum, and high-resolution spectra of B) Si 2p, C) N 1s, D) Cu 2p.

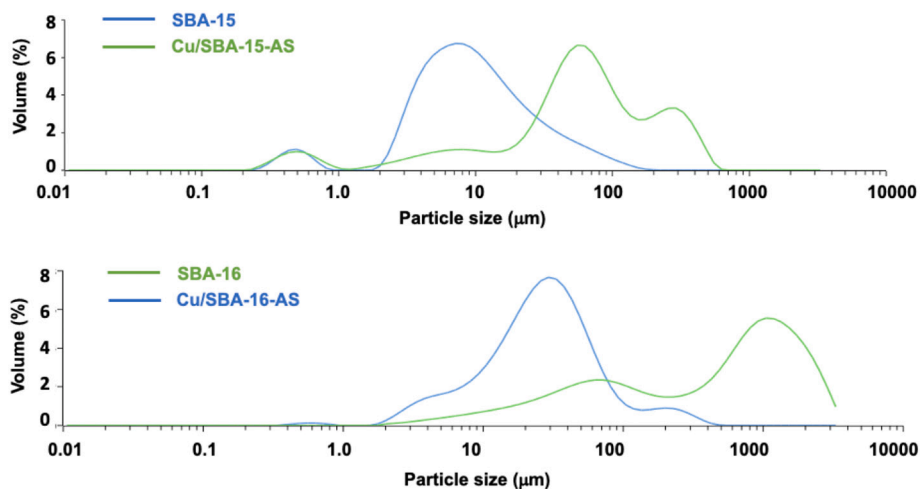


Fig. 6. Particle size distribution of modified and non-modified OMS.

This may be caused by the facility of attachment at the pore apertures. Consequently, the amine functional groups may block the micropores/small mesopores that lead to lessening in the surface area and pore volume [41]. Fig. S1 (Supporting Information) presents the nitrogen adsorption isotherms of non-modified and modified mesoporous silica samples. They belong to the IV type of isotherms according to the IUPAC classification characteristic for mesoporous materials [46].

Elemental analysis was used to identify the chemical compositions of materials obtained. It gave information about the content of nitrogen in the functionalized samples. These experiments were also carried out to

confirm the effectiveness of surface modification. The results were shown in Table 3. The contents of nitrogen, carbon, and hydrogen significantly increased in both aminosilane functionalized mesoporous silica compared to the pristine samples. It was also noticed that a higher amount of nitrogen was determined for Cu-SBA-15-AS that could have an influence on HCQ adsorption and release processes.

X-ray photoelectron spectroscopy enabled the determination of the chemical features of modified ordered mesoporous silica samples. The XPS surveys of Cu/SBA-15-AS and Cu/SBA-16-AS are depicted in Fig. 4A and Fig. 5A. In both spectra, intense peaks at around 530 eV assigned to

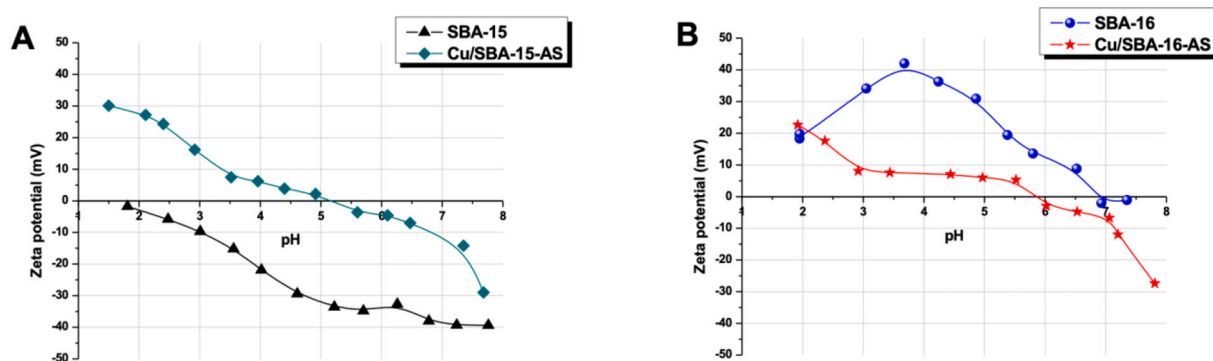


Fig. 7. Zeta potential vs. pH of SBA-15, Cu/SBA-15-AS (A) and SBA-16, Cu/SBA-16-AS (B).

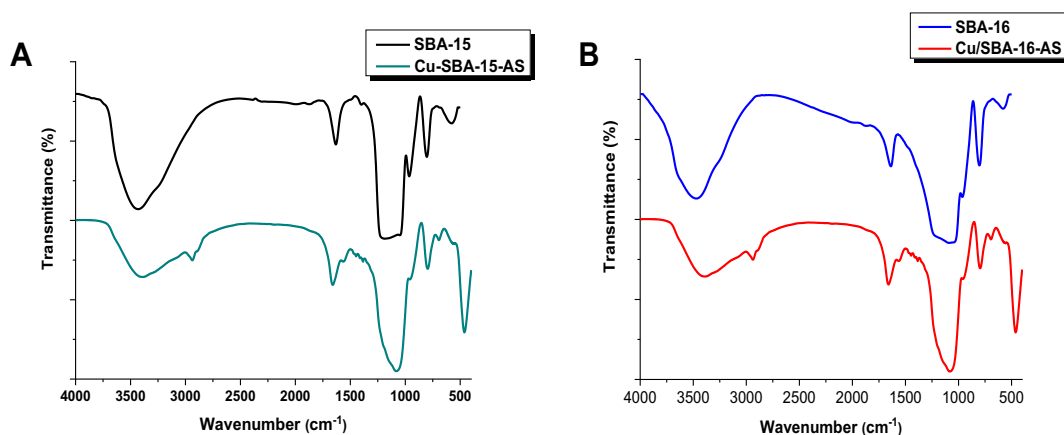


Fig. 8. FT-IR spectra of SBA-15, Cu/SBA-15-AS (A), SBA-16, and Cu/SBA-16-AS (B).

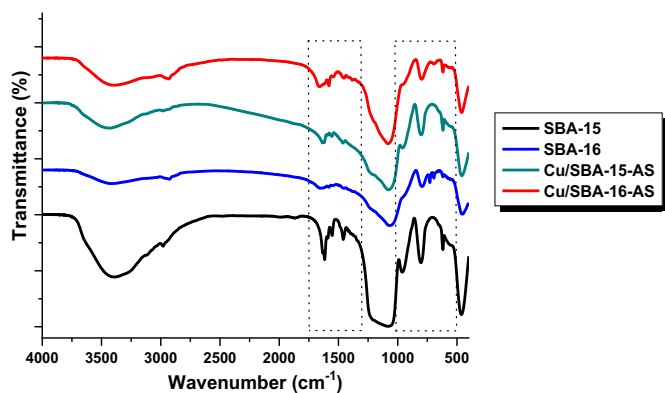


Fig. 9. FT-IR spectra of OMS materials after adsorption of HCQ.

oxygen were detected [47]. Additionally, the signals from Si 2p (103.3 eV, [48]), C 1s (286 eV, [49]) and N 1s (~400 eV, [50]) were determined. The small peaks derived from Cl 2p were also observed. Further analysis revealed that copper was present on the surface of both Cu/SBA-15-AS and Cu/SBA-16-AS. Based on the XPS survey it could be stated that the modification of pristine materials was effective.

Fig. 4B and Fig. 5B present also the high-resolution spectra of Si 2p. A single and symmetrical peak centered at about 103.3 eV was found in both cases. These results are characteristic of mesoporous silica materials and are in accordance with values reported in the literature [51–53]. The spectra of N 1s present the intense signals centered at about 400.4 eV for Cu/SBA-15-AS and at about 400.3 eV for Cu/SBA-16-AS which correspond to C-NH₂ in AS moiety (Fig. 4C and Fig. 5C).

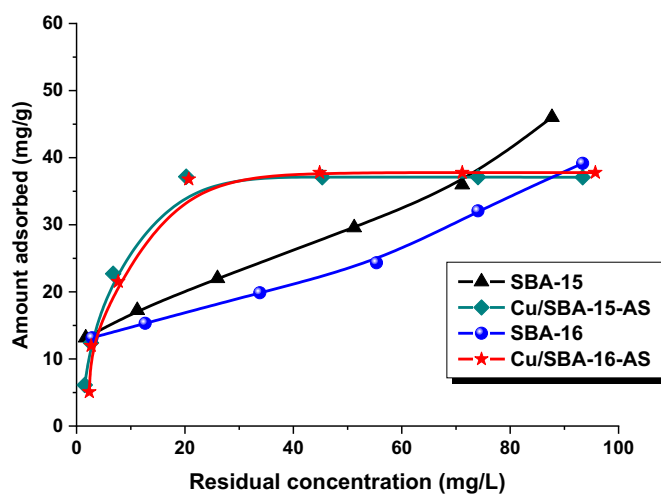


Fig. 10. Adsorption isotherms of HCQ on modified and non-modified OMS materials.

Furthermore, in order to determine the chemical state of copper in both modified samples, high-resolution XPS spectra were shown in Fig. 4D and Fig. 5D. The peaks located at binding energies of 933.7 eV and 953.5 eV (with relative intensity 2:1) are assigned to Cu 2p_{3/2} and 2p_{1/2}, respectively, that correspond to Cu(I). These results are in accordance with studies reported by Li et al. [54]. Additionally, two peaks at a binding energy of 936.3 eV and 956.5 eV were found in the spectrum that correspond to Cu 2p_{3/2} and Cu 2p_{1/2}, respectively, that are assigned

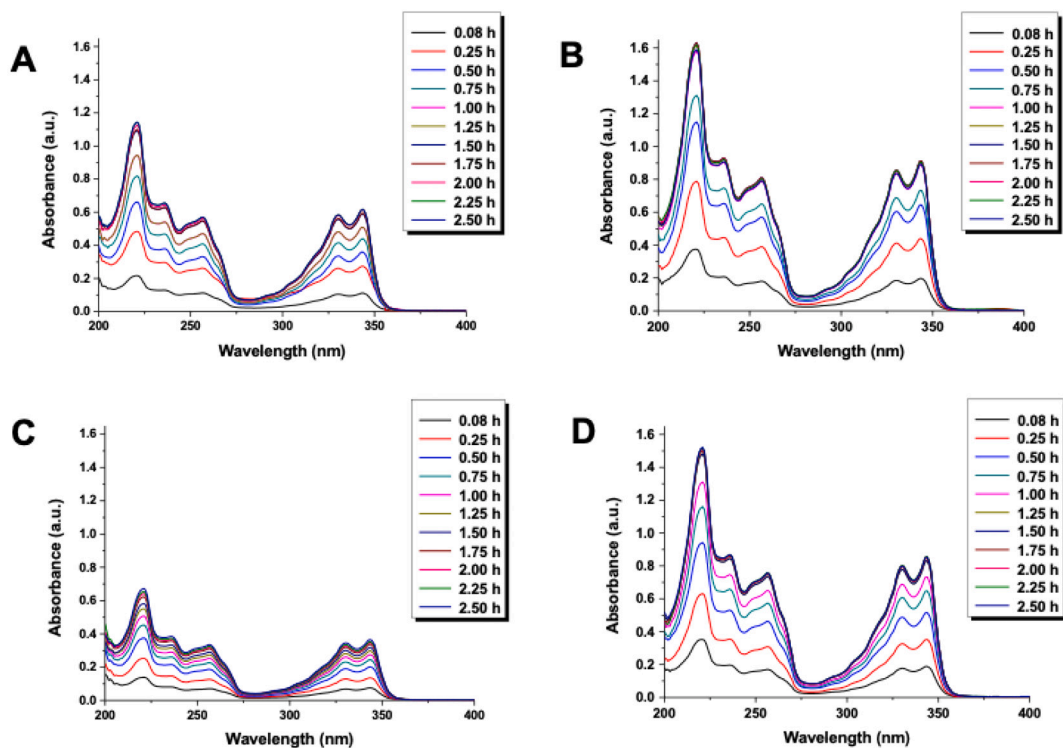


Fig. 11. UV spectra of HCQ released from SBA-15 (A), Cu/SBA-15-AS (B), SBA-16 (C), Cu/SBA-16-AS (D) over time at pH 7.2.

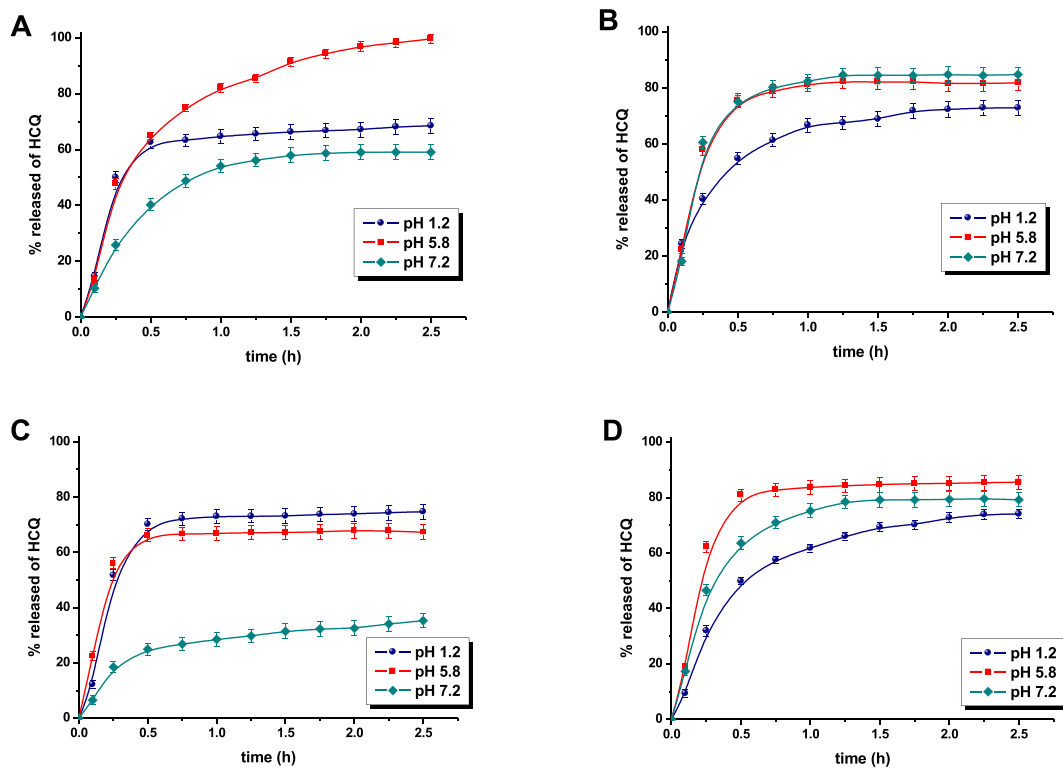


Fig. 12. Release profiles of HCQ from SBA-15 (A), Cu/SBA-15-AS (B), SBA-16 (C), Cu/SBA-16-AS.

to Cu(II) [55]. The existence of satellite peaks in the spectra was determined at 943.9 eV and 963.3 eV. The detailed spectral characteristics for the samples are presented in Supporting Information in Table S2. It should be highlighted that the determination of the chemical state of copper by XPS spectroscopy is challenging because Cu(0), Cu(I)

and Cu(II) can give signals in the same range of binding energies ($\sim 932\text{--}936$ eV) [56]. The decisive elements may be the line width or the appearance of strong satellites characteristic only for the Cu(II) state. In both Cu/SBA-15-AS and Cu/SBA-16-AS samples the presence of these satellites was observed. They could be assigned to the Cu^{II} signal because

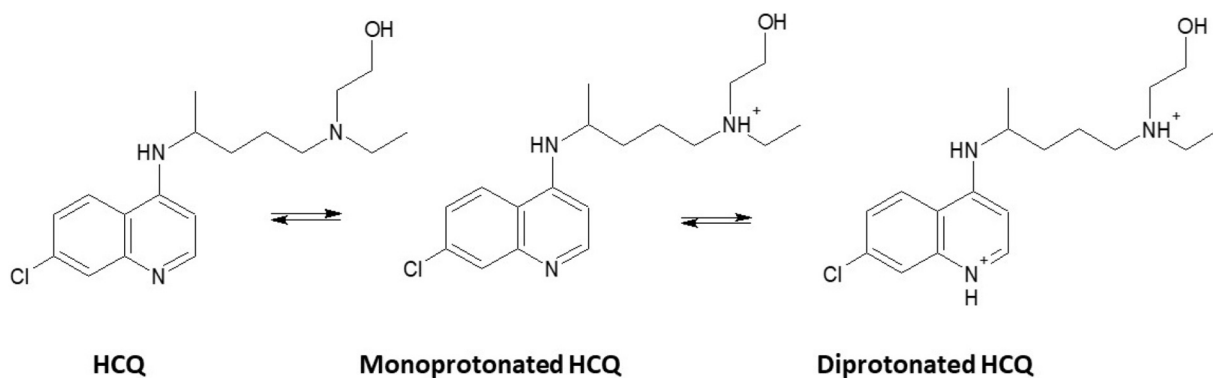


Fig. 13. Dissociation equilibrium of hydroxychloroquine (monoprotonated and diprotonated form of HCQ) [72].

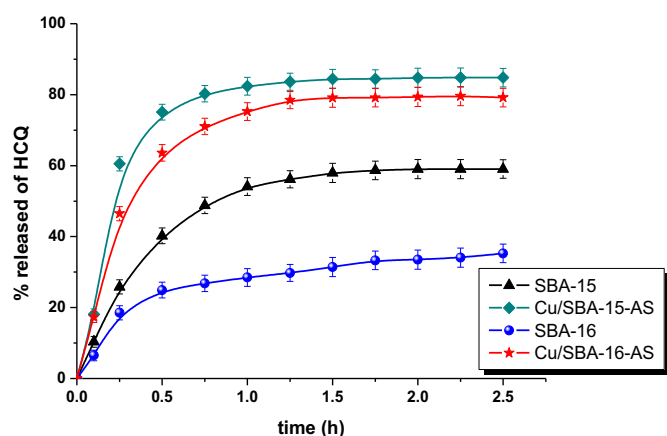


Fig. 14. Release profiles of HCQ from modified and non-modified mesoporous silica materials at pH 7.2.

changing in its intensity causes a change in the intensity of the satellites.

Additionally, the high-resolution XPS spectra of the O 1s, C 1s, Cl 2p for both modified materials are displayed in Figs. S2 and S3 (Supporting Information). The detailed spectral characteristics of the tested samples (quantitative and qualitative analysis) are presented in Table S2. The signal from O 1s was decomposed into two binding energy components (Figs. S2 A, S3 A). The peak with the highest atomic concentration at 532.8 eV is attributed to Si—O—Si [57]. The minor signal at 531.4 eV for Cu/SBA-15-AS and 531.2 eV for Cu/SBA-16-AS can be assigned to Si—O—H. In the case of Cu/SBA-15-AS (Fig. S2 B), the signal of C 1s was decomposed into three components. The main peak at 285.2 eV (25.4%) corresponds to C—C bonds [58,59] that are assigned to the propyl chain in the AS moiety. Another component determined at 286.5 eV (5.9%) is attributed to C—N [60]. The last C 1s peak at 288.8 eV (3.8%) originates from C—Si. It is supposed that due to the relationship between copper ions and AS moiety the binding energy was shifted. The same components were observed for Cu/SBA-16-AS (Fig. S3 B), however, the atomic concentrations were slightly different than for Cu/SBA-15-AS (Table S2). The Cl 2p XPS spectra in Fig. S2 C and Fig. S3 C exhibited a single peak centered at around 199.1 eV for Cu/SBA-15-AS and 199.2

eV for Cu/SBA-16-AS. It should be noted that the detected signal of chlorine was a residue after impregnation. The atomic concentration of Cl 2p was at a very low level for both samples.

The particle size distributions of OMS materials are depicted in Fig. 6. Particles with the smallest sizes (0.5 to 120 μm) were observed for SBA-15 of hexagonal structure. Its functionalization with APTES and impregnation with copper(II) chloride led to increasing in particle sizes (0.5 to 800 μm). Similar results were obtained for silica of cubic structure. The pristine SBA-16 had a relatively small particle size ranging from 2 to 700 μm , while modification of its surface with amine groups and copper ions caused a significant shift towards larger particle sizes. Table 4 shows the data in the form of $d(0.1)$, $d(0.5)$, $d(0.9)$, $D[3.2]$ and $D[4.3]$. The highest proportion of small particles was detected in SBA-15, while the greatest contribution of large particles was observed in the case of Cu/SBA-16-AS. The data obtained clearly indicated that the modification of both SBA-15 and SBA-16 materials with the APTES and copper ions led to the shifting of the PSD towards larger values.

Additionally, the zeta potential of modified and non-modified OMS at various pH was determined. Zeta potential gives information about the surface charge of selected nanomaterial that is useful to explain the behavior of samples at different conditions. It was observed that the zeta potential value of each silica material is strongly dependent on the pH of the medium (Fig. 7). For SBA-15 at pH value from 1.8 to 7.8 the electrokinetic potential was negative. It is suggested that Si—O⁻ species are formed because a proton detached from the silanol groups that are localized on the silica surface. Therefore, the pristine material of hexagonal structure acted as a weak acid [61]. After modification with aminosilane and impregnation with copper(II) chloride, the surface charge significantly changed. At pH ranging from 1.5 to 4.9 the zeta potential values were positive. It is assumed that NH₃⁺ species were formed because the aminosilane functional groups tend to gain proton. For Cu/SBA-15-AS the isoelectric point was reached at pH 5.2. From pH 5.3 to 7.8 the electrokinetic potential had negative values. It should be mentioned that colloidal systems are stable when zeta potential value is more than ± 25 mV [62]. Considering this principle, the pristine SBA-15 exhibited appropriate stability at pH ranging from 4.6 to 7.8, while the modified SBA-15 were stable at pH 1.5–2.4 and pH 7.7. For SBA-16 of cubic structure, the zeta potential values were positive from pH 2.0 to 6.6. Afterward, at pH 6.8 the isoelectric point was reached for this material. At pH higher than 7 the electrokinetic potential of SBA-16 was

Table 2

Textural parameters of SBA-15, Cu/SBA-15-AS, SBA-16, and Cu/SBA-16-AS materials.

Sample	BET surface area (m ² /g)	Total pore volume (cm ³ /g)	Average pore diameter (nm)
SBA-15	703	0.61	4.52
Cu/SBA-15-AS	282	0.42	6.65
SBA-16	727	0.25	2.84
Cu/SBA-16-AS	154	0.18	4.15

negative. It should be highlighted that only at pH ranging from 3 to 4.9 the colloidal system of SBA-16 was stable because the zeta potential values were higher than 25 mV. The different zeta potential profiles over the considered pH range for SBA-15 (hexagonal) and SBA-16 (cubic) could be explained by the distinction in their structure and the location of silanol groups that depending on the type of material can be present either within the pores of matrix or on the external surface. For Cu/SBA-16-AS the isoelectric point was shifted towards lower pH values compared to those obtained for SBA-16 sample and was reached at pH 5.8 (Fig. 7 B). The zeta potential values for Cu/SBA-16-AS were positive in the range of pH from 2 to 5.8. At pH higher than 6 the electrokinetic potential was negative due to possible electron donation interactions between Cu ions and aminosilane attached to the surface of materials. According to the theory regarding strong and weak acids and bases, copper ions exhibit tendency to bind with N atoms of amine groups [63].

The proposed mechanism for the formation of complexes between Cu (II) and aminosilane functionalized silica materials are presented in Fig. S4 (Supporting Information).

Fig. 8 shows FT-IR spectra of OMS materials synthesized in this study. The broad absorption band located in the 3750–3100 cm^{-1} that corresponds to the stretching vibrations of O—H and Si—OH bonds was detected in both pristine SBA-15 and SBA-16 samples. These results are in accordance with literature data in which silanol groups were detected in the range of 3730–3500 cm^{-1} [64]. In all four materials obtained the bending vibration of O—H bonds (at around 1640 cm^{-1}) and asymmetric stretching vibrations of Si—O—Si, Si—O—C and Si—C (at 1200–1100 cm^{-1}) were noted. Furthermore, the symmetrical stretching vibrations of Si—O—Si bonds at around 790 cm^{-1} were observed. It should be highlighted that for SBA-15 and SBA-16 free silanol groups located on surface were identified at 960 cm^{-1} . The intensity of this band in both modified materials was very low which suggested that the functionalization was successfully performed. In the spectra of Cu/SBA-15-AS and Cu/SBA-16-AS a band at around 1500 cm^{-1} attributed to N—H bending vibration was detected. Another evidence that the surface of materials was successfully modified is the diminution in the intensity of the band at approximately 3600 cm^{-1} assigned to the O—H stretching vibration. In the spectra of both copper ions and aminosilane functionalized OMS, a new band at around 2900 cm^{-1} was noticed that corresponded to C—H stretching vibrations of aliphatic chain which proved that the APTES was attached to the surface of materials. These results are consistent with data obtained in other studies [41,66]. The region around 3300 cm^{-1} and 3290 cm^{-1} is characteristic for asymmetric and symmetric stretching modes of NH_2 [67]. Additionally, the C—N stretching vibration should be detected in the wavenumber of range 1000–1200 cm^{-1} . However, it was overlapped with Si—O—Si, Si—O—C and Si—C found at 1200–1100 cm^{-1} . Another confirmation that the amine groups were attached to the surface of silica materials is a weak

peak at 673 cm^{-1} that corresponds to the bending of N—H bond [68].

In order to confirm that the HCQ was efficiently adsorbed on the surface of OMS, FT-IR spectra of organic-inorganic hybrid systems were recorded (Fig. 9). This technique enables to study intermolecular interactions between drug and nanomaterials. Apart from bands characteristic for silica materials which were mentioned above, the characteristic peaks of HCQ were found in the FT-IR spectra. The band at around 1611 cm^{-1} was assigned to the axial deformation of the C=N and C=C bonds of aromatic ring. Approximately at 1650–1550 cm^{-1} the N—H bond of secondary amine was recognized. At 1580 cm^{-1} and 1450 cm^{-1} the vibrations assigned to aromatic ring of HCQ were also recorded. The presence of tertiary amine was evidenced by bands at 1210–1150 cm^{-1} related to C—N stretching bond [69]. The peak located between 1177 and 1386 cm^{-1} was assigned to the S=O bonds of the sulfate [36]. The stretching bands of C—N in the regions 1360–1310 cm^{-1} overlapped by bands at 1350–1280 cm^{-1} were originated from aromatic tertiary and secondary amine, respectively. Additionally, the specific bands of carbon-halogen (C—Cl) between 550 and 850 cm^{-1} were also noted in FT-IR spectra of hybrid organic-inorganic system.

The pristine silica and their modified analogues were used as adsorbents for hydroxychloroquine. The chemical structure and geometric properties of HCQ were presented in Table 1. The isotherms of HCQ adsorbed on the surface of mesoporous materials are depicted in Fig. 10. It was observed that at low initial drug concentrations (from 3.125 to 50 mg/dm^3) the modification of OMS with aminosilane and copper ions significantly increased their sorption capacity compared to pristine samples. At low HCQ concentrations the active sites of Cu/SBA-15-AS and Cu/SBA-16-AS were highly accessible for drug loading and its adsorption was random. With increase in HCQ concentration, the drug molecules were tightly packed on the surface of modified OMS. At high hydroxychloroquine concentration the sorption capacity was constant because all available active sites were occupied either by drug molecules that could compete with each other or with water molecules. It is suggested that Cu^{2+} ions present on the surface of modified materials can generate complexes with HCQ. Lewis acid/base adducts are formed between copper ions and hydroxychloroquine. Based on the computational approaches performed by Rezaee et al. [70], it is assumed that complexes can be generated near the electron rich sites in HCQ molecules such as N—, O— and Cl— groups. It is expected that these sites may donate the lone pairs to 3d and 4s orbital of copper atoms. Furthermore, the N of pyridine ring and oxygen of hydroxyl group of HCQ will have the highest affinity to interact with Cu^{2+} ions of modified silica materials.

The shape of adsorption isotherms of both modified materials Cu/SBA-15-AS and Cu/SBA-16-AS proved that monolayer coverage of HCQ was formed on their surfaces. These results are consistent with other studies performed with the use of HCQ [71]. It should be added that the mechanism of HCQ binding to silica carriers can be based on the formation of hydrogen bonds between N—H groups of HCQ and O—H groups of pristine material. Additionally, a hydrogen bond can be created between O—H of HCQ and N—H of APTES modified material. The FT-IR spectra proved that interactions between functionalized silica and drug occurred. Before HCQ adsorption a band at around 1500 cm^{-1} of N—H groups was detected and after its loading the intensity of band was significantly reduced. Similar attractions between molecules were observed when magnetic metal-organic frameworks were applied for

Table 3
Elemental analysis of materials obtained.

Sample	N (%)	C (%)	H (%)	S (%)
SBA-15	0.016	0.841	1.519	0
Cu-SBA-15-AS	5.885	16.560	5.112	0.017
SBA-16	0.001	0.298	2.150	0.004
Cu-SBA-16-AS	3.212	12.430	3.606	0.012

Table 4
Particle size distribution of modified and non-modified mesoporous silica materials.

Sample	d (0.1) (μm)	d (0.5) (μm)	d (0.9) (μm)	D[3.2] (μm)	D[4.3] (μm)
SBA-15	3.15 \pm 0.08	8.84 \pm 0.12	36.42 \pm 2.51	4.25 \pm 0.58	15.70 \pm 1.14
Cu/SBA-15-AS	4.92 \pm 0.13	59.70 \pm 3.15	277.13 \pm 4.12	6.22 \pm 0.89	101.00 \pm 2.78
SBA-16	6.54 \pm 0.23	26.30 \pm 1.43	75.40 \pm 2.39	13.80 \pm 1.23	40.40 \pm 1.89
Cu/SBA-16-AS	25.20 \pm 1.08	557.00 \pm 10.12	1930.00 \pm 16.00	60.70 \pm 0.08	765.00 \pm 11.10

extraction of HCQ [72]. On the other hand, the drug loading efficiency depends to a large extent on textural features such as pore volume, pore diameter and surface properties of mesoporous materials [73]. It can be observed that the total pore volume of materials was a crucial parameter that had influence on hydroxychloroquine loading. These results are consistent with literature data [74]. The highest amount of HCQ was adsorbed on SBA-15 with the highest pore volume (0.61 cm³/g) compared to other silica materials obtained. Therefore, for this sample, multilayer adsorption can take place. This can be an explanation why the saturation in the case of non-modified materials was not observed. The total pore volume of SBA-16 was 0.25 cm³/g consequently the drug loading was lower than for silica of hexagonal structure. In turn, the functionalization with aminosilane and then impregnation with copper (II) chloride reduced significantly both the BET surface area and total pore volume and thus the HCQ loading capacity at high drug concentration was lower compared to non-modified analogues. It was possible to determine the maximum sorption capacities for Cu/SBA-15-AS and Cu/SBA-16-AS, which were 37.1 mg/g and 37.7 mg/g, respectively.

The release studies of HCQ from OMS materials were performed in three media simulating gastric fluid (pH 1.2), intestinal fluid (pH 5.8) and saliva (pH 7.2). In order to calculate the percentage of HCQ released from each mesoporous silica, initially the UV spectra at certain interval of time were recorded and the results obtained at pH 7.2 were presented in Fig. 11. The data registered at pH 5.8 were depicted in Fig. S5 (Supporting Information). It can be observed that depending on the type of material applied the absorbance over time increased.

Based on these results the cumulative percent of drug released from modified and non-modified mesoporous silica was calculated and the graphs are presented in Fig. 12. It was observed that pH conditions had influence on the drug release profiles. For SBA-15 the highest cumulative release was achieved at pH 5.8, 99% of HCQ was detected in receptor fluid within 2.5 h (Fig. 12A). In turn, at pH 1.2 the initial burst release within first 30 min was noticed, followed by a steady diffusion that lasted till the end of experiment. The lowest amount of drug was released from SBA-15 at pH 7.2 (ca. 50%). This could be related to the fact that at physiological pH HCQ has a positive charge [75] while according to the zeta potential measurements, SBA-15 has a negative charge on its surface. Therefore, it could be suggested that interactions between drug and nanomaterial were based on attractions of organic and inorganic components of hybrid system. The cumulative release of HCQ at pH 7.2 was much lower compared to other media conditions because the interactions between HCQ and SBA-15 were stronger than those obtained at another pH, so hydroxychloroquine could not be easily released to the receptor fluid. It should be also added that depending on pH values different ionization forms of HCQ can be created (Fig. 13). Hydroxychloroquine is a weak base that accumulates within acidic lysosomes [76,77]. There are three basic functional groups in the structure of HCQ with pK_a values below 4.00, 8.27, and 9.67 [78]. Hydroxychloroquine is fully protonated at low pH (around 4) as H₂HCQ²⁺, while

at neutral conditions there are two types of species protonated H₂HCQ²⁺ (ca. 66%) and monoprotonated HHCQ⁺ (ca. 34%). Whereas in alkaline solution, the proportion of HHCQ⁺ significantly increased to ca. 83%. At high pH there is also HCQ in its neutral form [79]. According to Parvinzadeh and Daneshfar [80] the pH value of the medium has an influence on the adsorption mechanism of HCQ. It was observed that at acidic condition the nitrogen atoms of hydroxychloroquine and the amino groups of APTES attached to the surface of silica materials were protonated, and the formation of hydrogen bonds was hindered. At a higher pH value, the hydrogen bond formation was enhanced, because other hydroxychloroquine species were also present than at lower pH [72]. Therefore, it is suggested that these electrostatic attractions may affect the release of active compound from OMS materials. This phenomenon was noticed when pristine materials (SBA-15 and SBA-16) were applied as vehicles for HCQ. At pH 7.2 the lowest amount of drug was released from non-modified silica. Due to the formation of hydrogen bonds between N–H groups of HCQ and surface silanol groups of SBA-15 and SBA-16 the diffusion of drug molecules was hindered.

The diffusion profiles of hydroxychloroquine after modification of SBA-15 with APTES and copper(II) chloride were different than those achieved using the pristine material. The release curves of HCQ at pH 5.8 and pH 7.2 were very similar and were overlapping each other. At pH 1.2 the release amount of drug was much lower. The different release profiles at various pH conditions might be related to the surface charge of the modified material. The surface of Cu/SBA-15-AS at low pH had positive charge, while at pH 5.8 and pH 7.2 had negative charge (Fig. 7A). Additionally, the formation of complex between drug molecules and copper ions present on the surface of modified mesoporous materials may have influence on the HCQ release profiles.

The amount of drug diffused from pristine and modified SBA-16 was different than that achieved for mesoporous silicas of SBA-15 type. It is suggested that for Cu/SBA-16-AS the hydroxychloroquine release was affected not only by the surface charge of materials at various pH conditions but also by specific interactions that are formed between copper ions, aminosilane groups and HCQ (Fig. 12).

Additionally, the influence of material type on the drug release process was also discussed. For this purpose, the obtained results were presented at different pH conditions for all synthesized OMS. The release profiles of HCQ at pH 1.2 (Fig. S6 A, Supporting Information) were very similar regardless of the type of silica material used. At pH 5.8 the highest amount of drug was released from SBA-15 and the lowest from SBA-16. For both modified materials Cu/SBA-15-AS and Cu/SBA-16-AS similar HCQ dissolution profile was noticed (Fig. S6 B, Supporting Information). The biggest differences in the HCQ release profiles were found at pH 7.2 (Fig. 14). This could be related not only to the surface charge of these materials but also to their textural properties and the type of their structure. It can be perceived that at pH 7.2 the lowest amount of HCQ was released from SBA-16. Negatively charged surface of SBA-16 interacted with diprotonated HCQ and therefore drug

Table 5
Kinetic models applied to describe the release of HCQ from mesoporous materials.

Sample	pH	Zero order		First order		Higuchi		Hixson-Crowell		Korsmeyer-Peppas		Type of transport
		R ²	k ₀ (h ⁻¹)	R ²	k ₁ (h ⁻¹)	R ²	k _H (h ^{-1/2})	R ²	k _{HC} (h ^{-1/3})	R ²	n	
SBA-15	1.2	0.677	7.82	0.736	0.20	0.775	16.31	0.716	0.23	0.842	0.132	quasi-Fickian
Cu/SBA-15-AS		0.826	18.39	0.879	0.40	0.898	32.57	0.856	0.45	0.952	0.368	quasi-Fickian
SBA-16		0.499	10.38	0.508	0.24	0.586	18.32	0.493	0.26	0.723	0.160	quasi-Fickian
Cu/SBA-16-AS	5.8	0.825	37.92	0.895	0.57	0.932	44.69	0.869	0.77	0.942	0.375	quasi-Fickian
SBA-15		0.905	25.91	0.985	1.53	0.968	52.23	0.989	1.26	0.992	0.297	quasi-Fickian
Cu/SBA-15-AS		0.606	12.68	0.688	0.75	0.717	50.23	0.588	0.65	0.849	0.187	quasi-Fickian
SBA-16	7.2	0.536	6.79	0.551	0.18	0.615	10.94	0.511	0.16	0.751	0.092	quasi-Fickian
Cu/SBA-16-AS		0.534	11.17	0.633	0.82	0.659	53.15	0.549	0.71	0.752	0.144	quasi-Fickian
SBA-15		0.781	16.87	0.834	0.32	0.883	34.95	0.817	0.40	0.919	0.389	quasi-Fickian
Cu/SBA-15-AS	7.2	0.698	13.57	0.736	0.47	0.809	26.99	0.678	0.90	0.885	0.167	quasi-Fickian
SBA-16		0.909	8.61	0.926	0.12	0.929	14.66	0.794	0.24	0.971	0.280	quasi-Fickian
Cu/SBA-16-AS		0.774	19.51	0.806	0.50	0.873	38.29	0.796	0.87	0.922	0.272	quasi-Fickian

diffusion was limited. Moreover, it was found that higher amount of drug was released from modified silica materials compared to the pristine samples. The initial burst release was detected within 1 h of the experiment. It is expected that due to the presence of copper ions and amino-functional groups on Cu/SBA-16-AS, the HCQ was mainly adsorbed on the outer surface of silica. These findings were also proved in other studies performed by Song et al. [81]. It should be noted that the total surface area of SBA-16 was higher than that of hexagonal material SBA-15. This finding could have also influence on its better sorption capacity and thus it had impact on drug release. Higher amount of HCQ was released from SBA-15 compared to SBA-16 due to the difference in pore diameter. The material of hexagonal structure was characterized by larger pore diameter (4.52 nm) than material of cubic structure (2.84 nm). When pores are larger, higher amount of hydroxychloroquine was released because the interactions between walls of material and drug molecules were weaker.

Five mathematical models were used to fit the experimental data of HCQ release from non-modified and modified OMS materials. In Table 5, the calculated kinetic values of release constants (k), correlation coefficients (R^2) and release exponent (n) were presented. The graphs presenting the fitting of HCQ release data to kinetic models are included in Supporting Information (Figs. S7–S9). For all materials obtained and, in all media applied, the highest R^2 values were achieved for Korsmeyer-Peppas model. The n values were below 0.5 that indicated quasi-Fickian drug transport. Similar results were obtained when hydroxychloroquine was released from Fe₃O₄ nanoparticles [82].

3. Conclusions

The results obtained proved that the modification of mesoporous silica with APTES and impregnation with copper(II) chloride was successfully achieved. Based on SAXS profiles and TEM images it can be stated that pristine SBA-15 and SBA-16 had highly ordered mesoporous structures. In turn, for the aminosilane and copper(II) chloride modified materials the degree of mesostructure ordering decreased. A similar relationship was observed in the case of textural parameters. OMS modification significantly reduced their specific surface area and pore volume. The obtained data revealed that the adsorption process of HCQ was more efficient on the surface of modified materials only at low drug concentrations. It was found that pore volume is the crucial parameter that had influence on the sorption capacity. The highest amount of HCQ was adsorbed on SBA-15 with the largest pore volume (0.614 cm³/g) compared to other OMS materials synthesized. The release behavior of HCQ from mesoporous silica nanocarriers was highly determined by the pH conditions and it could be regulated by the introduction of functional groups on the surface of materials. The release of drug from OMS was best fitted to Korsmeyer-Peppas model and the release mechanism followed Fickian diffusion.

The presented study is crucial to understand the relationship between the physicochemical properties of mesoporous silica nanocarriers and antiviral drug molecules. The proposed delivery systems can be successfully applied in any antiviral therapy. It should be noted that despite the development of various types of vaccines, in the long term, finding appropriate antiviral drugs incorporated into carriers designed using nanotechnological solutions will be a priority. Especially considering the rate at which viruses mutate. The appropriately selected antiviral drug delivery system can reduce the frequency of drug daily dosage and in this way decrease its toxicity. Therefore, synthesized OMS can be used as a smart vehicle for HCQ that will allow a controlled release of the antiviral drug at the chosen location of the body. It is expected that introduction of copper on the surface of mesoporous materials will enhance their antiviral and antibacterial activity. The biological studies will be performed in the future.

CRedit authorship contribution statement

Anna Olejnik: Investigation, Writing – original draft, Visualization.
Joanna Goscianska: Conceptualization, Investigation, Writing – original draft, Supervision, Writing – review & editing.

Declaration of competing interest

The authors declare that they have no known competing financial interests or personal relationships that could have appeared to influence the work reported in this paper.

Acknowledgements

Financial support from Polish Ministry of Science and Higher Education is acknowledged.

Appendix A. Supplementary data

Supplementary data to this article can be found online at <https://doi.org/10.1016/j.msec.2021.112438>.

References

- [1] K.D. Rainsford, A.L. Parke, M. Clifford-Rashotte, W.F. Kean, Therapy and pharmacological properties of hydroxychloroquine and chloroquine in treatment of systemic lupus erythematosus, rheumatoid arthritis and related diseases, *Inflammopharmacology*. 23 (2015) 231–269.
- [2] I. Ben-Zvi, S. Kivity, P. Langevitz, Y. Shoenfeld, Hydroxychloroquine: from malaria to autoimmunity, *Clin. Rev. Allergy Immunol.* 42 (2012) 145–153.
- [3] M.G. Tektonidou, L. Andreoli, M. Limper, Z. Amoura, R. Cervera, N. Costedoat-Chalumeau, M.J. Cuadrado, T. Dörner, R. Ferrer-Oliveras, K. Hambly, EULAR recommendations for the management of antiphospholipid syndrome in adults, *Ann. Rheum. Dis.* 78 (2019) 1296–1304.
- [4] M. Ramos-Casals, P. Brito-Zerón, S. Bombardieri, H. Bootsma, S. De Vita, T. Dörner, B.A. Fisher, J.-E. Gottenberg, G. Hernandez-Molina, A. Kocher, EULAR recommendations for the management of Sjögren's syndrome with topical and systemic therapies, *Ann. Rheum. Dis.* 79 (2020) 3–18.
- [5] E. Pauli, H. Joshi, A. Vasavada, J. Brackett, L. Towa, Evaluation of an immediate-release formulation of hydroxychloroquine sulfate with an interwoven pediatric taste-masking system, *J. Pharm. Sci.* 109 (2020) 1493–1497.
- [6] P.S. Akhavan, J. Su, W. Lou, D.D. Gladman, M.B. Urowitz, P.R. Fortin, The early protective effect of hydroxychloroquine on the risk of cumulative damage in patients with systemic lupus erythematosus, *J. Rheumatol.* 40 (2013) 831–841.
- [7] S. Das, K.R. Anu, S. Birangal, S. Akbar, B. Ahmed, A. Joseph, The controversial therapeutic journey of chloroquine and hydroxychloroquine in the battle against SARS-CoV-2: a comprehensive review, *Med. Drug Discov.* 10 (2021), 100085.
- [8] C. Wright, C. Ross, N. Mc Goldrick, Are hydroxychloroquine and chloroquine effective in the treatment of SARS-COV-2 (COVID-19)? *Evid. Based. Dent.* 21 (2020) 64–65.
- [9] H. Akpovwa, Chloroquine could be used for the treatment of filoviral infections and other viral infections that emerge or emerged from viruses requiring an acidic pH for infectivity, *Cell Biochem. Funct.* 34 (2016) 191–196.
- [10] A. Kumar, B. Liang, M. Aarthi, S.K. Singh, N. Garg, I.U. Mysorekar, R. Giri, Hydroxychloroquine inhibits Zika virus NS2B-NS3 protease, *ACS Omega*. 3 (2018) 18132–18141.
- [11] J. Lajoie, L. Mwangi, K.R. Fowke, Preventing HIV infection without targeting the virus: how reducing HIV target cells at the genital tract is a new approach to HIV prevention, *AIDS Res. Ther.* 14 (2017) 1–5.
- [12] P. Kronenberg, R. Vrijns, A. Boeyé, Chloroquine induces empty capsid formation during poliovirus eclipse, *J. Virol.* 65 (1991) 7008–7011.
- [13] E.E. Ooi, J.S.W. Chew, J.P. Loh, R.C.S. Chua, In vitro inhibition of human influenza A virus replication by chloroquine, *Virol. J.* 3 (2006) 39, <https://doi.org/10.1186/1743-422X-3-39>.
- [14] D.L. Barnard, C.W. Day, K. Bailey, M. Heiner, R. Montgomery, L. Lauridsen, P.K. S. Chan, R.W. Sidwell, Evaluation of immunomodulators, interferons and known in vitro SARS-coV inhibitors for inhibition of SARS-coV replication in BALB/c mice, *Antivir. Chem. Chemother.* 17 (2006) 275–284.
- [15] E.S. Rosenberg, E.M. Dufort, T. Udo, L.A. Wilberschied, J. Kumar, J. Tesoriero, P. Weinberg, J. Kirkwood, A. Muse, J. DeHovitz, Association of treatment with hydroxychloroquine or azithromycin with in-hospital mortality in patients with COVID-19 in New York State, *Jama*. 323 (2020) 2493–2502.
- [16] S. Arshad, P. Kilgore, Z.S. Chaudhry, G. Jacobsen, D.D. Wang, K. Huitsing, I. Brar, G.J. Alangaden, M.S. Ramesh, J.E. McKinnon, Treatment with hydroxychloroquine, azithromycin, and combination in patients hospitalized with COVID-19, *Int. J. Infect. Dis.* 97 (2020) 396–403.
- [17] Z. Chen, J. Hu, Z. Zhang, S. Jiang, S. Han, D. Yan, R. Zhuang, B. Hu, Z. Zhang, Efficacy of hydroxychloroquine in patients with COVID-19: results of a randomized clinical trial, *Medrxiv* (2020), <https://doi.org/10.1101/2020.03.22.20040758>.

- [18] W.H. Self, M.W. Semler, L.M. Leither, J.D. Casey, D.C. Angus, R.G. Brower, S. Y. Chang, S.P. Collins, J.C. Eppensteiner, M.R. Filbin, Effect of hydroxychloroquine on clinical status at 14 days in hospitalized patients with COVID-19: a randomized clinical trial, *JAMA*. 324 (2020) 2165–2176.
- [19] J. Geleris, Y. Sun, J. Platt, J. Zucker, M. Baldwin, G. Hripesak, A. Labella, D. K. Manson, C. Kubin, R.G. Barr, Observational study of hydroxychloroquine in hospitalized patients with Covid-19, *N. Engl. J. Med.* 382 (2020) 2411–2418.
- [20] C. Biot, W. Daher, N. Chavain, T. Fandeur, J. Khalife, D. Dive, E. De Clercq, Design and synthesis of hydroxyferroquine derivatives with antimalarial and antiviral activities, *J. Med. Chem.* 49 (2006) 2845–2849.
- [21] M.L. Estes, D. Ewing-Wilson, S.M. Chou, H. Mitsumoto, M. Hanson, E. Shirey, N. B. Ratliff, Chloroquine neurotoxicity. Clinical and pathologic perspective, *Am. J. Med.* 82 (1987) 447–455.
- [22] H.N. Bernstein, Ocular safety of hydroxychloroquine sulfate (Plaquenil), *South. Med. J.* 85 (1992) 274–279.
- [23] A. Srinivasa, S. Tosounidou, C. Gordon, Increased incidence of gastrointestinal side effects in patients taking hydroxychloroquine: a brand-related issue? *J. Rheumatol.* 44 (2017) 398.
- [24] I.H. Yusuf, S. Sharma, R. Luqmani, S.M. Downes, Hydroxychloroquine retinopathy, *Eye*. 31 (2017) 828–845.
- [25] X. Yao, F. Ye, M. Zhang, C. Cui, B. Huang, P. Niu, X. Liu, L. Zhao, E. Dong, C. Song, In vitro antiviral activity and projection of optimized dosing design of hydroxychloroquine for the treatment of severe acute respiratory syndrome coronavirus 2 (SARS-CoV-2), *Clin. Infect. Dis.* 71 (2020) 732–739.
- [26] Ö. Kutlu, A. Metin, A case of exacerbation of psoriasis after oseltamivir and hydroxychloroquine in a patient with COVID-19: will cases of psoriasis increase after COVID-19 pandemic? *Dermatol. Ther.* 33 (2020) e13383.
- [27] S. Wang, Ordered mesoporous materials for drug delivery, *Microporous Mesoporous Mater.* 117 (2009) 1–9.
- [28] J. Goscianska, A. Olejnik, I. Nowak, M. Marciniak, R. Pietrzak, Ordered mesoporous silica modified with lanthanum for ibuprofen loading and release behaviour, *Eur. J. Pharm. Biopharm.* 94 (2015), <https://doi.org/10.1016/j.ejpb.2015.07.003>.
- [29] Y. Zhu, J. Shi, W. Shen, X. Dong, J. Feng, M. Ruan, Y. Li, Stimuli-responsive controlled drug release from a hollow mesoporous silica sphere/polyelectrolyte multilayer core-shell structure, *Angew. Chem.* 117 (2005) 5213–5217.
- [30] D. Shao, F. Zhang, F. Chen, X. Zheng, H. Hu, C. Yang, Z. Tu, Z. Wang, Z. Chang, J. Lu, Biomimetic diselenide-bridged mesoporous organosilica nanoparticles as an X-ray-responsive biodegradable carrier for chemo-immunotherapy, *Adv. Mater.* 32 (2020), 2004385.
- [31] L. Pan, Q. He, J. Liu, Y. Chen, M. Ma, L. Zhang, J. Shi, Nuclear-targeted drug delivery of TAT peptide-conjugated monodisperse mesoporous silica nanoparticles, *J. Am. Chem. Soc.* 134 (2012) 5722–5725.
- [32] J. Lee, J.R. Prohaska, D.J. Thiele, Essential role for mammalian copper transporter Ctr1 in copper homeostasis and embryonic development, *Proc. Natl. Acad. Sci.* 98 (2001) 6842–6847.
- [33] C.D. Sifri, G.H. Burke, K.B. Enfield, Reduced health care-associated infections in an acute care community hospital using a combination of self-disinfecting copper-impregnated composite hard surfaces and linens, *Am. J. Infect. Control* (2016), <https://doi.org/10.1016/j.ajic.2016.07.007>.
- [34] S.L. Warnes, E.N. Summersgill, C.W. Keevil, Inactivation of murine norovirus on a range of copper alloy surfaces is accompanied by loss of capsid integrity, *Appl. Environ. Microbiol.* (2015), <https://doi.org/10.1128/AEM.03280-14>.
- [35] K. Malachová, P. Praus, Z. Rybková, O. Kozák, Antibacterial and antifungal activities of silver, copper and zinc montmorillonites, *Appl. Clay Sci.* 53 (2011) 642–645.
- [36] A.N.F. Moraes, L.A.D. Silva, M.A. de Oliveira, E.M. de Oliveira, T.L. Nascimento, E. M. Lima, I.M.S. Torres, D.G.A. Diniz, Compatibility study of hydroxychloroquine sulfate with pharmaceutical excipients using thermal and nonthermal techniques for the development of hard capsules, *J. Therm. Anal. Calorim.* (2019) 1–10.
- [37] Y. Li, M.H. Cho, S.S. Lee, D.-E. Lee, H. Cheong, Y. Choi, Hydroxychloroquine-loaded hollow mesoporous silica nanoparticles for enhanced autophagy inhibition and radiation therapy, *J. Control. Release* 325 (2020) 100–110.
- [38] F. Ciesielczyk, L. Klapiszewski, K. Szwarz-Rzepka, T. Jesionowski, A novel method of combination of Kraft lignin with synthetic mineral support, *Adv. Powder Technol.* 25 (2014) 695–703.
- [39] J. Goscianska, I. Nowak, A. Olejnik, Sorptive properties of aluminium ions containing mesoporous silica towards l-histidine, *Adsorption*. 22 (2016), <https://doi.org/10.1007/s10450-015-9727-z>.
- [40] A. Olejnik, I. Nowak, G. Schroeder, Functionalized polystyrene beads as carriers in release studies of two herbicides: 2,4-dichlorophenoxyacetic acid and 2-methyl-4-chlorophenoxyacetic acid, *Int. J. Environ. Sci. Technol.* 16 (2019), <https://doi.org/10.1007/s13762-018-2138-4>.
- [41] J. Goscianska, A. Olejnik, I. Nowak, APTES-functionalized mesoporous silica as a vehicle for antipyrine – adsorption and release studies, *Colloids Surfaces A Physicochem. Eng. Asp.* 533 (2017), <https://doi.org/10.1016/j.colsurfa.2017.07.043>.
- [42] M. Kruk, M. Jaroniec, C.H. Ko, R. Ryoo, Characterization of the porous structure of SBA-15, *Chem. Mater.* 12 (2000) 1961–1968.
- [43] R.A. Sacramento, O.M.S. Cysneiros, B.J.B. Silva, A.O.S. Silva, Synthesis and characterization of mesoporous materials with SBA and MCM structure types, *Cerâmica*. 65 (2019) 585–591.
- [44] M.A. Ballem, J.M. Córdoba, M. Odén, Influence of synthesis temperature on morphology of SBA-16 mesoporous materials with a three-dimensional pore system, *Microporous Mesoporous Mater.* 129 (2010) 106–111.
- [45] T.M. Albayati, Application of nanoporous material MCM-41 in a membrane adsorption reactor (MAR) as a hybrid process for removal of methyl orange, *Desalin. Water Treat.* 151 (2019) 138–144.
- [46] K.A. Cychosz, M. Thommes, Progress in the physisorption characterization of nanoporous gas storage materials, *Engineering*. 4 (2018) 559–566.
- [47] L.Q. Wu, Y.C. Li, S.Q. Li, Z.Z. Li, G.D. Tang, W.H. Qi, L.C. Xue, X.S. Ge, L.L. Ding, Method for estimating ionicities of oxides using O1s photoelectron spectra, *AIP Adv.* 5 (2015) 97210.
- [48] H. Darmstadt, C. Roy, S. Kaliaguine, S.J. Choi, R. Ryoo, Surface chemistry of ordered mesoporous carbons, *Carbon* 40 (2002) 2673–2683. N. Y.
- [49] D. Fang, F. He, J. Xie, L. Xue, Calibration of binding energy positions with C1s for XPS results, *J. Wuhan Univ. Technol. Sci. Ed.* 35 (2020) 711–718.
- [50] P. Rechnia-Gorący, A. Malaika, M. Kozłowski, Acidic activated carbons as catalysts of biodiesel formation, *Diam. Relat. Mater.* 87 (2018) 124–133.
- [51] M. Gómez-Cazalilla, J.M. Mérida-Robles, A. Gurbani, E. Rodríguez-Castellón, A. Jiménez-López, *J. Solid State Chem.* 180 (2007) 1130.
- [52] W. Xu, T. Ollevier, F. Kleitz, Iron-modified mesoporous silica as an efficient solid Lewis acid catalyst for the Mukaiyama Aldol reaction, *ACS Catal.* 8 (2018) 1932–1944.
- [53] E.P. Reddy, L. Davydov, P.G. Smirniotis, Characterization of titania loaded V-, Fe-, and Cr-incorporated MCM-41 by XRD, TPR, UV–vis, Raman, and XPS techniques, *J. Phys. Chem. B* 106 (2002) 3394–3401.
- [54] H. Li, M. Yang, X. Zhang, L. Yan, J. Li, Y. Qi, Mesoporous silica-supported copper-catalysts for homocoupling reaction of terminal alkynes at room-temperature, *New J. Chem.* 37 (2013) 1343–1349.
- [55] C. Huo, J. Ouyang, H. Yang, CuO nanoparticles encapsulated inside Al-MCM-41 mesoporous materials via direct synthetic route, *Sci. Rep.* 4 (2014) 1–9.
- [56] M.C. Biesinger, Advanced analysis of copper X-ray photoelectron spectra, *Surf. Interface Anal.* 49 (2017) 1325–1334.
- [57] P. Post, L. Wurlitzer, W. Maus-Friedrichs, A.P. Weber, Characterization and applications of nanoparticles modified in-flight with silica or silica-organic coatings, *Nanomaterials*. 8 (2018) 530.
- [58] J. Ederer, P. Janoš, P. Ecorchard, J. Tolasz, V. Štengl, H. Beneš, M. Perchacz, O. Pop-Georgievski, Determination of amino groups on functionalized graphene oxide for polyurethane nanomaterials: XPS quantitation vs functional speciation, *RSC Adv.* 7 (2017) 12464–12473.
- [59] M.Y. Bashouti, Y. Paska, S.R. Puniredd, T. Stelzner, S. Christiansen, H. Haick, Silicon nanowires terminated with methyl functionalities exhibit stronger Si-C bonds than equivalent 2D surfaces, *Phys. Chem. Chem. Phys.* 11 (2009) 3845–3848.
- [60] A. Wach, P. Natkański, M. Drozdek, B. Dudek, P. Kuśrowski, Functionalization of mesoporous SBA-15 silica by grafting of polyvinylamine on epoxy-modified surface, *Polimery*. 62 (2017) 516–524.
- [61] E. Papirer, *Adsorption on Silica Surfaces*, CRC Press, 2000.
- [62] J. Goscianska, A. Olejnik, I. Nowak, M. Marciniak, R. Pietrzak, Stability analysis of functionalized mesoporous carbon materials in aqueous solution, *Chem. Eng. J.* 290 (2016), <https://doi.org/10.1016/j.cej.2016.01.060>.
- [63] W. Nowicki, Structural studies of complexation of Cu(II) with aminosilane-modified silica surface in heterogeneous system in a wide range of pH, *Appl. Surf. Sci.* 469 (2019) 566–572.
- [64] S.-W. Song, K. Hidajat, S. Kawi, pH-controllable drug release using hydrogel encapsulated mesoporous silica, *Chem. Commun.* (2007) 4396–4398.
- [65] G.M. Ziarani, A. Badieli, S. Mousavi, N. Lashgari, A. Shahbazi, Application of amino-functionalized SBA-15 type mesoporous silica in one-pot synthesis of spirooxindoles, *Chin. J. Catal.* 33 (2012) 1832–1839.
- [66] N. Majoul, S. Aouida, B. Bessais, Progress of porous silicon APTES-functionalization by FTIR investigations, *Appl. Surf. Sci.* 331 (2015) 388–391.
- [67] A.S. Maria Chong, X.S. Zhao, Functionalization of SBA-15 with APTES and characterization of functionalized materials, *J. Phys. Chem. B* 107 (2003) 12650–12657.
- [68] J. Coates, Interpretation of infrared spectra, a practical approach, *Encycl. Anal. Chem. Appl. Theory Instrum.* (2006) 1–22.
- [69] P. Rezaee, M. Akbari, R. Morad, A. Koochaki, M. Maaz, Z. Jamshidi, First principle simulation of coated hydroxychloroquine on Ag, Au and Pt nanoparticle as a potential candidate for treatment of SARS-CoV-2 (COVID-19), in: *ArXiv Prepr. ArXiv2006.02343*, 2020.
- [70] H. Bendjeflal, M. Ziati, A. Aloui, H. Mamine, T. Metidji, A. Djebli, Y. Bouhedja, Adsorption and removal of hydroxychloroquine from aqueous media using Algerian kaolin: full factorial optimisation, kinetic, thermodynamic, and equilibrium studies, *Int. J. Environ. Anal. Chem.* (2021) 1–22.
- [71] F. Parvinzadeh, A. Daneshfar, Fabrication of a magnetic metal-organic framework molecularly imprinted polymer for extraction of anti-malaria agent hydroxychloroquine, *New J. Chem.* 43 (2019) 8508–8516.
- [72] N. Lang, A. Tuel, A fast and efficient ion-exchange procedure to remove surfactant molecules from MCM-41 materials, *Chem. Mater.* 16 (2004) 1961–1966.
- [73] P. Horcajada, A. Ramila, J. Perez-Pariente, M. Vallet-Regí, Influence of pore size of MCM-41 matrices on drug delivery rate, *Microporous Mesoporous Mater.* 68 (2004) 105–109.
- [74] J. Goscianska, R. Pietrzak, Removal of tartrazine from aqueous solution by carbon nanotubes decorated with silver nanoparticles, *Catal. Today* (2015), <https://doi.org/10.1016/j.cattod.2014.11.017>.
- [75] M.A.A. Al-Bari, Chloroquine analogues in drug discovery: new directions of uses, mechanisms of actions and toxic manifestations from malaria to multifarious diseases, *J. Antimicrob. Chemother.* 70 (2015) 1608–1621.

- [77] K.P. Collins, K.M. Jackson, D.L. Gustafson, Hydroxychloroquine: a physiologically-based pharmacokinetic model in the context of cancer-related autophagy modulation, *J. Pharmacol. Exp. Ther.* 365 (2018) 447–459.
- [78] R.I. Fox, Mechanism of action of hydroxychloroquine as an antirheumatic drug, in: *Semin. Arthritis Rheum.*, Elsevier, 1993, pp. 82–91.
- [79] D.C. Warhurst, J.C.P. Steele, I.S. Adagu, J.C. Craig, C. Cullander, Hydroxychloroquine is much less active than chloroquine against chloroquine-resistant *Plasmodium falciparum*, in agreement with its physicochemical properties, *J. Antimicrob. Chemother.* 52 (2003) 188–193.
- [80] S. Babić, D. Dabić, L. Ćurković, Fate of Hydroxychloroquine in the Aquatic Environment, 2017.
- [81] S.-W. Song, K. Hidajat, S. Kawi, Functionalized SBA-15 materials as carriers for controlled drug delivery: influence of surface properties on matrix–drug interactions, *Langmuir*. 21 (2005) 9568–9575.
- [82] M.S. Sadr, A. Heydarinasab, H.A. Panahi, R.S. Javan, Production and characterization of biocompatible nano-carrier based on Fe₃O₄ for magnetically hydroxychloroquine drug delivery, *Polym. Adv. Technol.* 32 (2021) 564–573, <https://doi.org/10.1002/pat.5110>.